THE JOURNAL OF PHYSICAL CHEMISTRY C

Article

Cite This: J. Phys. Chem. C 2019, 123, 22775−22786

pubs.acs.org/JPCC

First-Principles Studies of the Lithiation and Delithiation Paths in Si Anodes in Li-Ion Batteries

Kwai S. Chan,*[,†] Wu-Wei Liang,[†] and Candace K. Chan*[,‡]

[†]Materials Engineering Department, Mechanical Engineering Division, Southwest Research Institute, 6220 Culebra Road, San Antonio, Texas 78238, United States

[‡]Materials Science and Engineering School for Engineering of Matter, Transport and Energy, Arizona State University, 501 East Tyler Mall, ECG 301, Tempe, Arizona 85287-8706, United States

ABSTRACT: Understanding the lithiation of Si and the resulting formation of amorphous lithium silicides (a-Li_xSi) has been the subject of numerous studies due to the importance of silicon anodes for next-generation, high-energy-density lithium batteries. Experimental studies have shown that a-Li_xSi with $2 \leq x \leq 3.75$ appears as a prominent phase in the phase transformations of Si during lithiation and delithiation, but computational studies have yet to elucidate why. In this work, first-principles molecular dynamics computations were performed to simulate the various immediate steps associated with lithiation and delithiation of Si anodes in a Li-ion half-cell battery. The energy of formation and unit cell volume for relevant Li_xSi phases and Si have been computed for both crystalline and amorphous states. The first-principles results are utilized to construct lithiation and delithiation pathways and compute the corresponding changes in the voltage, capacity, and cell volume of the anode. These results indicate that multiple pathways are possible during delithiation of c-$Li_{15/4}Si$ and a two-phase delithiation field is energetically favored to occur between a-$Li_{15/4}Si$ and a-$Li_{9/4}Si$ due to a large amorphization energy for Li_3Si and a site-dependent amorphization energy for $Li_{9/4}Si$. In addition, large tensile stresses are generated during the removal of Li atoms from the 48e sites in the $Li_{15/4}Si$ crystalline lattice. These hydrostatic tensile stresses can cause changes to the open-circuit potential, can lead to the fracture of Si or $Li_{15}Si_4$, and may be responsible for the change in the lithiation process from a ledge mechanism to a two-phase mechanism at $x \approx 2.25$.

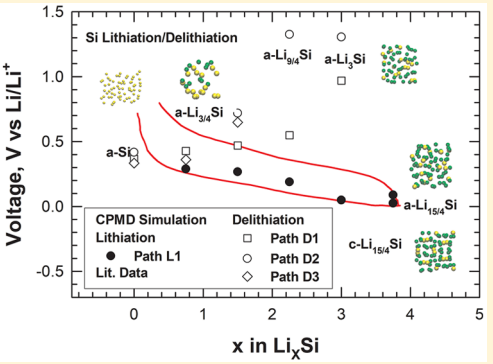

1. INTRODUCTION

Current Li-ion batteries based on graphitic anodes have a theoretical capacity of only 372 mAh/g. To improve battery performance, there is a need for higher specific capacity materials to increase the energy density of Li-ion batteries. Silicon is a particularly attractive anode material for Li-ion batteries because it has a theoretical charge storage capacity of about 3579 mAh/g, which is almost 10 times that of graphite.[1] However, the reversible reaction of lithium with silicon is accompanied by large changes in volume in excess of 300%.[2] This increase in volume can induce large lithiation stresses,[3] which cause significant parts of the electrode to contract[4] and crack, leading to particle motions.[5] These particle displacements can cause parts of the electrode to become electronically isolated and, hence, not able to participate in the charge storage reactions. Theoretical studies on electrodes made of Si particles have found that in order for the particles to be adequately spaced from each other in order to avoid displacement they must occupy only 20 vol % of the electrode, whereas the remaining mass consists of the binder and conducting additives.[6] Because the active Si material makes up such a small percentage of the electrode, this is a serious reduction in energy density. Mixing or ball-milling the Si with binders or other networking agents such as carbon nanotubes[7−9] has not completely solved these problems as the volume changes are too large for adequate binding.

To solve the decrepitation problem, several electrode morphologies and architectures have been explored in order to relax the strain and accommodate the volume changes without subsequent pulverization.[10] The terminal particle size phenomenon describes the critical size characteristic for each material that can withstand a given amount of strain without pulverizing. Particles below this size do not fracture further.[10] Experiments on lithium alloy electrodes have shown that electrochemical cycling is significantly improved if the initial particle size is very small,[11] consistent with the terminal particle size phenomenon. Promising results have been demonstrated by using nanostructured thin films,[12,13] particles,[12] porous structures,[14] pillars,[15] or nanowires.[16,17] All of these structures have been designed to allow room for volume expansion and relaxation of the triaxial tensile stresses. Long-term cycling (>100 cycles) at capacities close to the theoretical capacity of Si have yet to be demonstrated because the problem associated with the large volume change has not

Received: June 21, 2019
Revised: August 25, 2019
Published: August 26, 2019

DOI: 10.1021/acs.jpcc.9b05933
J. Phys. Chem. C 2019, 123, 22775−22786

been completely resolved, although progress has been made on several fronts.[18−20] By constraining the outer wall and directing the volume of expansion inward, long-term cycling of double-walled silicon nanotube electrodes in the range of 600−1000 mAh/g has been demonstrated for 6000 cycles.[18,19]

The lithiation of crystalline Si (c-Si) or amorphous Si (a-Si) at room temperature results in the formation of amorphous lithium silicide (a-Li_xSi) at the reaction front. In situ atomic force microscopy (AFM) studies[21] of the lithiation process of a-Si thin films have revealed that a-Si can be lithiated with large volume changes without pulverization or cracking when the a-Si particles are below a critical size and have sufficient space between particles to accommodate volume expansion. A number of electrochemical studies[22−31] including the use of in situ X-ray diffraction techniques[24,25] have shown that the lithiation of c-Si to a-Li_xSi occurs via a two-phase reaction.[6] Sloped features associated with two different single-phase regions were observed in the voltage curves during lithiation of c-Si with characteristic peaks in the differential capacity vs voltage curves (dQ/dV vs V plots).[23] An in situ Mössbauer study[26] revealed that the transition between the two single-phase regions, which occurred at about $Li_{2.3}Si$, corresponded to the structural state where added Li atoms would have only Li nearest neighbors and a chemical potential close to that of Li metal. A subsequent in situ transmission electron microscopy (TEM) study[27] of the dynamic lithiation process in single-crystal Si revealed a sharp interface on the order of 1 nm between c-Si and an a-Li_xSi phase. The lithiation process is controlled by the migration of the interface, which occurs by lateral movement of ledges formed on the interface. Lithiation by movement of ledges located on a sharp interface was also observed in another in situ TEM study by J. W. Wang et al.[28] during lithiation of a-Si to a-Li_xSi when x was about 2.5. Besides $x = 2.5$, x has also been reported by others to be as low as 2.17[29] to as high as 2.90[30]−3.5.[25] On the other hand, the two-phase reaction observed in the study of J. W. Wang et al.,[28] which was conducted under high charging rates (≫1C), was not supported by the study of Xu Wang et al.,[31] who reported only single-phase lithiation under conventional charging rates (<1C). At voltages below ∼30−60 mV vs Li/Li^+,[23,24] a-$Li_{15/4}Si$ can transform rapidly to c-$Li_{15/4}Si$ through a congruent transformation process.[25] During delithiation, c-$Li_{15/4}Si$ delithiates immediately to form an amorphous phase with $x \approx 2$ (a-Li_2Si) coexisting with c-$Li_{15/4}Si$ via a two-phase reaction process.[6,32] According to Gauthier et al.,[32] who measured the local Li compositions in a-Li_xSi using an ex situ electron energy loss spectroscopy technique,[32] local compositions between a-$Li_{15/4}Si$ and a-Li_2Si were never observed, but it is unclear why.

Complementary to experimental studies, several recent studies applied ab initio methods to evaluate the theoretical performance of electrode materials,[33] including simulating the Li insertion and deinsertion processes in c-Si,[34,35] a-Si,[36−39] and Si nanowires.[40,41] In particular, ab initio methods have been utilized to compute the energy of formation,[34−39] the electronic structure,[34,36−39,41,42] the open-circuit potential,[33−37] the volume change,[35,38,39] the diffusion path,[43,44] the amorphization process[43] of the lithiated phases, as well as the change of elastic properties,[38,39] and the role of stresses during lithiation.[44,45] To model solid-state amorphization of Li_xSi during lithiation of Si at room temperature, Chevrier and Dahn[36] performed density functional theory (DFT) calculations using the local density approximation. The lithiation process in Si was simulated by inserting a Li atom in the center of the largest spherical void among the neighboring Si atoms. For delithiation, a Li atom was removed randomly from Li_xSi. The lithiation algorithm developed by Chevrier and Dahn[36] was later adopted by Chan et al.[43] to model the lithiation and amorphization of c-Si single crystals with three different facet planes including (001), (110), and (111). Pan et al.[44] utilized ab initio molecular dynamics (MD) to investigate the effects of hydrostatic stresses on the Li diffusion process in a-LiSi. Their results showed that the presence of stress can alter Li diffusion by an order of magnitude either by increasing the free volume under tension or by changing the local structure under compression. These authors focused on a-LiSi only and did not investigate any other compositions. Jung et al.[46] performed reactive force field (ReaxFF) MD simulations of the lithiation and delithiation of silicon nanowires (SiNWs). Their simulation results showed that the delithiation process in SiNWs occurred via a two-phase mechanism involving c-Si and a-Li_xSi below a composition of $Li_{3/2}Si$. In a separate ReaxFF MD study,[47] Kim et al. showed that the delithiation response of an alumina-coated Si thin film is sensitive to the delithiation rate. Specifically, a fast delithiation rate led to the formation of porosity inside of a-Li_xSi, while a slow delithiation rate allowed a-Li_xSi to shrink to a nearly Li-free structure (a-$Li_{1/5}Si$) without internal pore formation. However, none of the above-mentioned computational studies elucidated why a-Li_2Si is favored over other a-Li_xSi compositions in the range of $2 \leq x \leq 3.75$.

In this article, we report the results of a first-principles computational study of the lithiation and delithiation processes of Si electrodes for selected compositions ranging from Si to $Li_{15}Si_4$ with the aim to try to understand why the $x \approx 2$ composition of a-Li_xSi seems to be an important phase in the electrochemical reaction. Using the Car−Parrinello molecular dynamics (CPMD) method,[48,49] first-principles computational modeling has been performed to simulate the lithium insertion process at the atomistic (unit cell) scale and compute the corresponding intercalation potential (voltage), volume change, and theoretical fracture stress and strain of the lithiated compounds. The computational methodology has been utilized to analyze the lithiation and delithiation processes in the Si anode by computing the corresponding volume change, hydrostatic stresses, and open-circuit potential at selected Li_xSi compositions in the range of $0 \leq x \leq 3.75$. These results show that large hydrostatic tensile stresses are generated when Li atoms are extracted from the unit cell of $Li_{15/4}Si$, in accordance with previous studies.[4,20] The hydrostatic tensile stresses are sufficiently high to cause changes to the open-circuit potential and fracture of Si or Li_xSi. The results suggest that a-Li_2Si is favored over a-Li_3Si because of a lower amorphization energy, showing that insights gained from the Si anode modeling may be utilized to develop a better understanding of the phase transformations in Si during lithiation and delithiation.

2. COMPUTATIONAL DETAILS

2.1. Car−Parrinello Molecular Dynamics Methods. The silicon lithiation and delithiation processes were modeled by computing the energy of formation of the lithiated compounds as a function of lithium content. The energy calculations were performed using an ab initio MD code, the CPMD method,[48] which is a plane wave implementation of DFT.[49] It uses an approximation frozen-core approach in which only the chemically active valence electrons are dealt

DOI: 10.1021/acs.jpcc.9b05933
J. Phys. Chem. C 2019, 123, 22775−22786

with explicitly and the inert core electrons are considered frozen together with the nuclei as rigid nonpolarizable ion cores. It is capable of both first-principles wave function optimization (static calculation) and ab initio MD calculations. For crystalline solids, the energy and equilibrium lattice constant of a unit cell at ground state (0 K) were computed by calculating the energies for unit cells with different lattice constants by performing wave function optimization with CPMD. A high-order (e.g., fourth-order) polynomial was fitted to the energy points. The equilibrium lattice constant was determined by finding the lattice constant corresponding to the minimum energy on the polynomial curve. For Si anodes, the lithiated compounds (Li_xSi) and the delithiated Si are often amorphous. To model this process, the energy of an amorphous phase was computed by heating the corresponding crystalline phase (Li_xSi and Si) above the melting point (2500 K), followed by rapid quenching to 300 K and holding at this temperature as a function of time to allow for atom relaxation and equilibrium to occur. A similar approach was utilized by Pan et al.[44] to model a-LiSi using VASP.[50]

The full lithiation of Si leads to a final product of c-$Li_{15}Si_4$ and a large volume expansion. To model this process, the CPMD method was also utilized to compute the theoretical stress−strain curves of Si and c-$Li_{15}Si_4$. For these computations, the optimized unit cell was pulled under triaxial tension by applying equal strains in the three principal crystallographic directions of the unit cell. The energy change was computed as a function of the applied strain. The derivative of the energy change with strain was performed to obtain the elastic constants, bulk modulus, and theoretical stress−strain curve, and the theoretical tensile strength was taken as the peak stress in the stress−strain curve.

2.2. Energy of Formation. First-principles computations were performed using the CPMD method[48,49] to determine the energy of formation for c-Si, Li, and c-$Li_{15}Si_4$ at the ground state (0 K). First, we built the unit cells of Si and Li and a supercell of $Li_{15}Si_4$, in which unit cells were diamond cubic ($Fd\bar{3}m$ space group), bcc, and simple cubic ($I\bar{4}3d$ space group),[34] respectively. The supercell of $Li_{15}Si_4$, which was comprised of four unit cells containing 60 Li atoms and 16 Si atoms ($Li_{60}Si_{16}$), was used to simulate delithiation by systematically reducing the number of Li atoms from the structure. The total energy for the unit cell of individual compounds or elements was computed and optimized as a function of the lattice constant. Similar computations were also performed using another first-principles computational code, called WIEN2K.[51] The total energy of an amorphous phase was computed using a computational annealing-and-quenching procedure[44] to vitrify a crystalline phase to an amorphous state at 300 K.

2.3. Computation of Lithiation Potential. The lithiation of Si to form Li_xSi is governed by the reaction given by eq 1[36,37]

$$\mathrm{Si} + x\mathrm{Li} \rightarrow \mathrm{Li}_x\mathrm{Si} \tag{1}$$

and the formation energy of the lithiated compound, Li_xSi, is obtained from the total energy, E_r, according to eq 2[36,37]

$$E_r(x) = E_r[\mathrm{Li}_x\mathrm{Si}] - (xE_r[\mathrm{Li}] + E_r[\mathrm{Si}]) \tag{2}$$

where $E_r[Z]$ denotes the internal energy of Z. The internal energy can be used to approximate the Gibbs free energy by ignoring the pressure and entropy terms.[33−36] The open-circuit potential vs Li of Li_xSi is given by eq 3[36,37]

$$V(x) = -\frac{1}{e}\frac{dE_r(x)}{dx} \tag{3}$$

where V is the potential and e is the electron charge. For lithiation of Li_xSi to form Li_ySi, the reaction proceeds according to eq 4

$$\mathrm{Li}_x\mathrm{Si} + (y - x)\mathrm{Li} \rightarrow \mathrm{Li}_y\mathrm{Si} \tag{4}$$

and the open-circuit voltage is given by eq 5[33,34]

$$V = \frac{E_r[\mathrm{Li}_x\mathrm{Si}] + (y - x)E_r[\mathrm{Li}] - E_r[\mathrm{Li}_y\mathrm{Si}]}{(y - x)F} \tag{5}$$

where $y - x$ is the charge on the lithium ion during the reaction ($y > x$); F is Faraday's constant, and $E_r(Z)$ with Z = Li_xSi, Li, or Li_ySi is the internal energy of Z that can be determined from first-principles computational methods. The hydrostatic stresses induced during lithiation and delithiation of Si can also induce a voltage gap. According to the analysis by Lu et al.,[45] the open-circuit voltage gap, V_s, induced by the hydrostatic stresses is given by eq 6[45]

$$V_s = \frac{\sigma_h\Omega}{F} \tag{6}$$

where σ_h is the hydrostatic stress, Ω is the partial molar volume, and F is the Faraday constant. If one considers the lithiation process to proceed according to eq 1 and the hydrostatic stress reached at the formation of c-$Li_{15/4}Si$ is designated as σ_h^*, the open-circuit voltage gap associated with the hydrostatic stress during the formation of Li_xSi is then given by eq 7

$$V_s = \frac{x\sigma_h(\mathrm{Li}_{15/4}\mathrm{Si})\Omega}{3.75F} \tag{7}$$

which can be combined with eq 2 to give eq 8

$$V = \frac{E_r[\mathrm{Li}_x\mathrm{Si}] + (y - x)E_r[\mathrm{Li}] - E_r[\mathrm{Li}_y\mathrm{Si}]}{(y - x)F} + \frac{x\sigma_h^*\Omega}{3.75F} \tag{8}$$

as the open-circuit voltage associated with the lithiation and delithiation processes of Si involving volumetric changes and the generation of hydrostatic residual stresses. To compute the hydrostatic stresses, the elastic constants (C_{ij}) and bulk moduli (B) of Si and $Li_{15}Si_4$ were required. The elastic constants C_{ij} and bulk moduli (B) of Si and c-$Li_{15}Si_4$ were computed using CPMD.

3. RESULTS

3.1. Simulation of Silicon and Lithium Silicide Structures. The lattice constants, a_o, of the equilibrium unit cells for c-Si, Li, and c-$Li_{15}Si_4$ calculated using CMPD and WIEN2K are compared in Table 1, showing good agreement between the two methods and those reported in the literature.[34,52−55]

The results of the computational annealing-and-quenching of c-Si and c-$Li_{15/4}Si$ are shown in Figure 1. For Si, the computational procedure involved heating a unit cell of c-Si, Figure 1a (bottom insert), to a temperature above the melting point (2500 K) to attain an amorphous structure and then quickly cooling down to 300 K to preserve the amorphous state, Figure 1a (top inset). The total energies/per atom of a-Si and c-Si were computed as a function of time until the atoms

DOI: 10.1021/acs.jpcc.9b05933
J. Phys. Chem. C 2019, 123, 22775−22786

Table 1. Equilibrium Lattice Constants for Bulk Crystalline Li, Si, and $Li_{15}Si_4$

		Si	Li	$Li_{15/4}Si$
a_0 (Å)	WIEN2K	5.48157	3.40175	10.5879
	CPMD	5.45566	3.44612	10.6417
	lit. values	5.451[52]	3.49[54]	10.60[34]
		5.44[53]		10.6852[55]

in the cluster were relaxed completely. The time step for the MD simulation was 0.0483 fs. The volume and total energy of the unit cell were computed during the entire relaxation process, and the relaxation simulation was terminated when the energy change of the current time step differed from the previous time step by less than 1×10^{-5} eV. The total energies/per atom for a-Si and c-Si are compared in Figure 1a, which shows that the total energy of a-Si exceeds that of c-Si by 0.188 eV. Thus, the amorphization energy of c-Si, ΔE_a, has a value of 0.188 eV. The total energy of c-Si was obtained by heating c-Si from 0 to 300 K.

Using the same procedure, the total energy of a-$Li_{15/4}Si$ was obtained by heating a supercell of c-$Li_{15/4}Si$ to a temperature above the melting point to attain an amorphous structure and then quickly cooling down to 300 K to preserve the amorphous state. The total energies/per atom of a-$Li_{15/4}Si$ and c-$Li_{15/4}Si$ were computed as a function of time until the atoms in the cluster were relaxed completely. As in the Si simulation, the time step for the MD simulation of a-$Li_{15/4}Si$ was 0.0483 fs. The volume and total energy of the supercell were computed during the entire relaxation process, and the relaxation simulation was terminated when the energy change of the current time step differed from the previous time step by less than 1×10^{-5} eV. The total energies/per atom for a-$Li_{15/4}Si$ and c-$Li_{15/4}Si$ are compared in Figure 1b, which shows that the total energy of a-$Li_{15/4}Si$ exceeds that of c-$Li_{15/4}Si$ by 0.235 eV.

CPMD simulations of Li extraction were performed by systematically removing Li atoms from specified lattice sites in a c-$Li_{15}Si_4$ supercell. Although not representative of the actual delithiation processes that occur in a Si-based anode, this approach enables a systematic evaluation of composition over a range of Li−Si ratios; moreover, the computation annealing-and-quenching procedure is expected to result in an amorphous structure from an initially crystalline structure of an identical composition, making it feasible to compare the relative energy of formation of an identical composition in the amorphous and crystalline states. In this study, the influence of the Li atom removal rate on the delithiation mechanisms of lithiated Si such as that investigated by Kim et al.[47] will not be considered because the delithiation rate is expected to have little or no impact on the energy of formation of Li_xSi compounds on the basis of thermodynamics considerations. However, the findings of Kim et al.[47] will be discussed in conjunction with the results of the current study in section 4.

A 4 × 4 supercell of $Li_{15}Si_4$ contains 60 Li atoms in two Wyckoff sites (12a sites and 48e sites) and 16 Si atoms at a third Wyckoff site (16c site), as shown in Table 2. In the

Table 2. Atom Locations and Fractional Coordinates of $Li_{15}Si_4$ with the Space Group of $I\bar{4}3d$[22,34]

Wyckoff site	(x, y, z)
Li(12a)	(0.375, 0.000, 0.250)
Li(48e)	(0.123, 0.154, 0.963)
Si(16c)	(0.458, 0.458, 0.458)

CPMD computation, a c-$Li_{15}Si_4$ supercell of four formula units ($Li_{60}Si_{16}$) in equilibrium was used as the starting point. Lithium delithiation from $Li_{15}Si_4$ to form Li_3Si was simulated by removing the 12 Li atoms from the 12a site ($Li_{60}Si_{16}$ − 12Li = Li_3Si). After Li extraction, the supercell containing just the filled 48e (Li) and 16c (Si) sites ($Li_{48}Si_{16}$ or Li_3Si) was allowed to relax at 300 K. The time step utilized in the MD simulation was 0.0483 fs. The volume and the total energy of the supercell were computed during the entire relaxation process until the computation process was terminated when the energy change between the current and the previous steps differed by less than 1×10^{-5} eV. The same conditions were applied to the other MD simulations described later in this paper.

Figure 2a shows the energy/Si atom of Li_3Si as a function of time. Subsequently, the Li_3Si cluster was heated to 2500 K (above the melting point of the silicide) to allow amorphization to occur. The silicide was then quenched rapidly to 300 K to preserve and then relax the a-Li_3Si structure. The energy change/Si atom of Li_3Si in the amorphous state is compared to that of the c-Li_3Si in Figure 2a. The comparison indicates that relaxed Li_3Si has a lower energy state than a-Li_3Si. In this figure, relaxed Li_3Si is labeled with the word "crystalline" in quotation marks because Li_3Si is initially crystalline, but it is uncertain that the intermediate phase (Li_3Si) is truly crystalline after relaxation of the atoms in

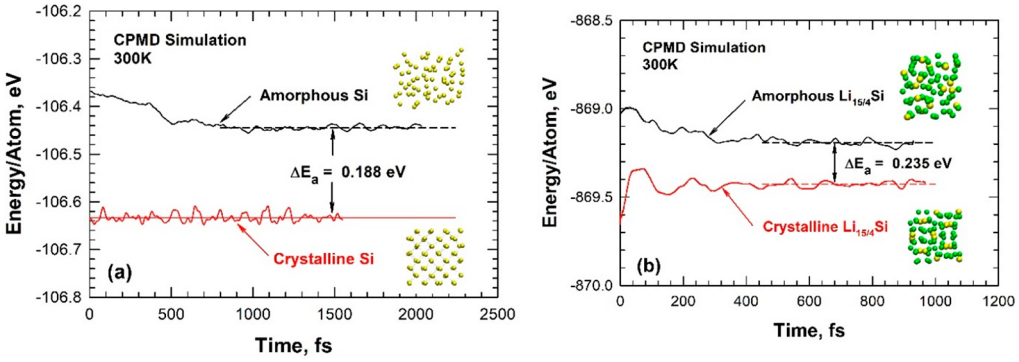

Figure 1. Energy/atom curves for c-Si and a-Si and $Li_{15}Si_4$: (a) energy/atom curve of c-Si compared to that of a-Si showing an energy difference of 0.188 eV; (b) energy/atom curve of c-$Li_{15/4}Si$ compared to that of a-$Li_{15/4}Si$ showing an energy difference of 0.235 eV. Amorphization of Si and $Li_{15}Si_4$ was simulated by heating and quenching the crystalline compound from the melting point (2500 K) to 300 K. The structures of the crystalline and amorphous compounds are shown as insets (yellow: Si; green: Li).

DOI: 10.1021/acs.jpcc.9b05933
J. Phys. Chem. C 2019, 123, 22775−22786

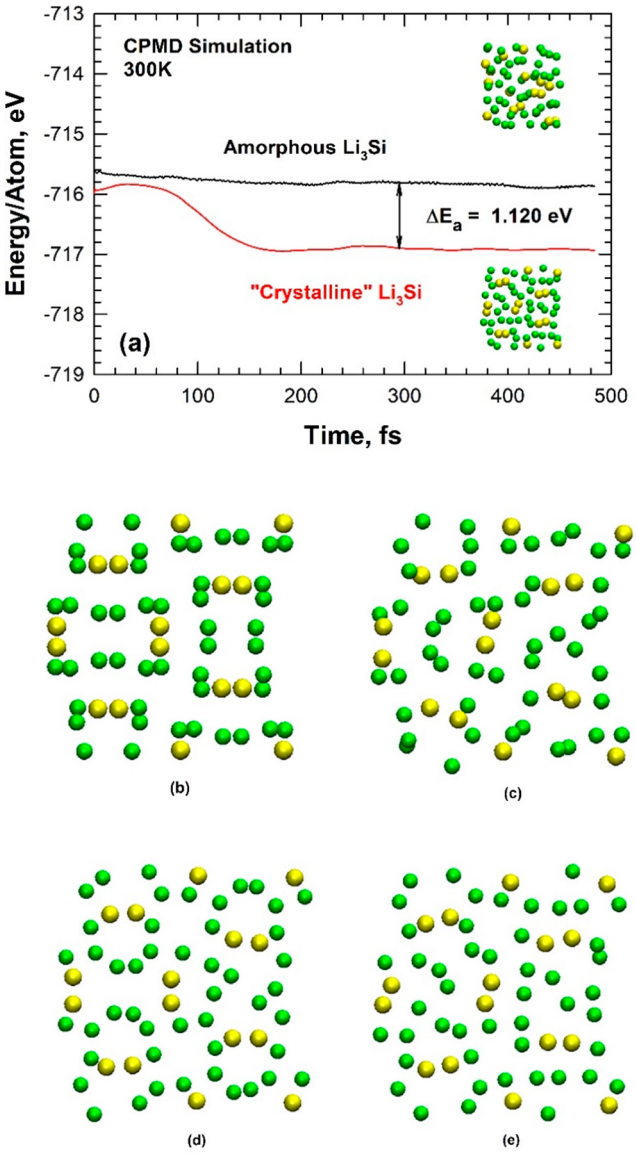

Figure 2. Amorphization of Li_3Si: (a) energy/Si atom curve of "crystalline" Li_3Si produced by extraction of 12 Li atoms from the 48e sites of a supercell of $Li_{15}Si_4$ compared to Li_3Si in an amorphous state produced by heating and quenching of "crystalline" Li_3Si produced by delithiation of $Li_{15}Si_4$; structure of Li_3Si after extraction of 12 Li atoms from $Li_{15}Si_4$ at various times of relaxation at 300 K: (b) 0, (c) 100, (d) 200, and (e) 400 fs (yellow: Si; green: Li).

the cluster because the corresponding radial distribution function analysis of the relaxed structure has not been performed. The atom positions of the relaxed structure are somewhat different from those of the initial c-Li_3Si structure, and they are also significantly different from those of the a-Li_3Si. Figure 2b–e shows the structures of Li_3Si at relaxation times of 0, 100, 200, and 400 fs, respectively.

A similar procedure was used to extract an additional 12 Li atoms from the 48e sites in order to simulate the delithiation of Li_3Si to form $Li_{36}Si_{16}$ ($Li_{48}Si_{16}$ − 12Li = $Li_{36}Si_{16}$ = $Li_{9/4}Si$). The energy change/Si atom of $Li_{9/4}Si$ in the amorphous state is compared to that of the c-$Li_{9/4}Si$ in Figure 3a. The energy curve for "c-$Li_{9/4}Si$" is depicted by the dashed curve. When the "c-$Li_{9/4}Si$" is amorphized by heating, the energy curve of the a-$Li_{9/4}Si$, shown as a solid curve, is increased and then decreased upon quenching to 300 K. After equalization and relaxation at 300 K, the energy curve for a-$Li_{9/4}Si$ reaches a relatively constant value with ΔE_a = 1.799 eV above that of the "c-$Li_{9/4}Si$", as shown in Figure 3a. The removal of an additional 12 Li atoms from $Li_{9/4}Si$ gives $Li_{24}Si_{16}$ ($Li_{36}Si_{16}$ − 12Li = $Li_{24}Si_{16}$ = $Li_{3/2}Si$), and the results for the energy change/Si are shown in Figure 3b. Like a-$Li_{9/4}Si$, the energy curve for a-$Li_{3/2}Si$ is higher than that for c-$Li_{3/2}Si$ by ΔE_a = 0.5717 eV.

Further removal of 12 atoms from $Li_{24}Si_{16}$ resulted in $Li_{12}Si_{16}$ ($Li_{3/4}Si$) with 12 Li atoms at the 48e site. The energy change/Si atom of $Li_{9/4}Si$ in the amorphous state is compared to that of the c-$Li_{3/4}Si$ in Figure 3c. Like a-$Li_{9/4}Si$ and a-$Li_{3/2}Si$, the energy curve for a-$Li_{3/4}Si$ shows a rise in the total energy once "c-$Li_{3/4}Si$" is heated up to 2500 K. After quenching to 300 K, the energy curve for a-$Li_{3/4}Si$ decreases to a ΔE_a of 2.473 × 10^{-3} eV, indicating a very small energy difference between "c-$Li_{3/4}Si$" and a-$Li_{3/4}Si$.

The final simulation of the delithiation process involved extraction of 48 Li atoms from c-$Li_{15}Si_4$ from the 48e sites ($Li_{60}Si_{15}$ − 48Li = $Li_{12}Si_{16}$ = $Li_{3/4}Si$ = $Li_{0.75}Si$) but with 12 Li atoms remaining at the 12a sites to form $Li_{12}Si_{16}$ ($Li_{3/4}Si$). After Li extraction, the unit cell with the remaining 12 Li atoms (at the 12a sites) and 16 Si atoms was allowed to relax at 300 K. Figure 3d shows the energy/Si atom of $Li_{3/4}Si$ as a function of time. Subsequently, the $Li_{3/4}Si$ unit cell was heated to 2500 K (above the melting point of the silicide) to allow amorphization to occur. The silicide was then quenched rapidly to 300 K to preserve and then relax the a-$Li_{3/4}Si$ structure. The energy change/Si atom of $Li_{3/4}Si$ in the amorphous state is compared to that of the "crystalline" $Li_{3/4}Si$ in Figure 3d. The comparison indicates that a-$Li_{3/4}Si$ has a higher energy state than "c-$Li_{3/4}Si$" when the Li atoms are at the 12a sites. Combined with the finding shown in Figure 3c, it becomes apparent that the amorphization energy of c-$Li_{3/4}Si$ is not a constant but depends on the Wyckoff sites (i.e., 12a sites or 48e sites) where the Li atoms are located. Figure 4 shows the structure of $Li_{3/4}Si$ at several times of relaxation. A comparison of the size of the unit cell at t = 0 in Figure 4a and at t = 100 fs in Figure 4b revealed that a large volume shrinkage occurred when the 48 Li atoms were removed from the 48e sites while with 12 Li atoms situated at the 12a sites. Figure 4c,d shows local rearrangements of Li and Si atoms for relaxation times of 200 and 400 fs, respectively. At these relaxation times, no significant volume shrinkages were observed in the relaxed structures compared to that shown in Figure 4b for 100 fs.

3.2. Formation Energy and Lithiation/Delithiation Pathways. The CPMD energy results were utilized to obtain the energy of formation for the c-Li_xSi and a-Li_xSi compounds. These results are summarized in Table 3. The volume of the unit cell associated with individual c-Li_xSi and a-Li_xSi compounds was computed at the equilibrium configuration as part of the delithiation simulation, and the results are also presented in Table 3.

Table 3 shows a summary of the relative energy levels of various Li_xSi compounds in the crystalline and amorphous states. The results in Table 3 have been utilized to construct potential lithiation and delithiation paths considering the energy formation/Si atoms when the Li content is increased (lithiation) or decreased (delithiation). The energies of formation for a-Si and c-Si are compared against those for a-Li_xSi and c-Li_xSi as a function of the unit cell volume to the 1/3 power in Figure 5a. For all c-Li_xSi compounds, the energies

DOI: 10.1021/acs.jpcc.9b05933
J. Phys. Chem. C 2019, 123, 22775−22786

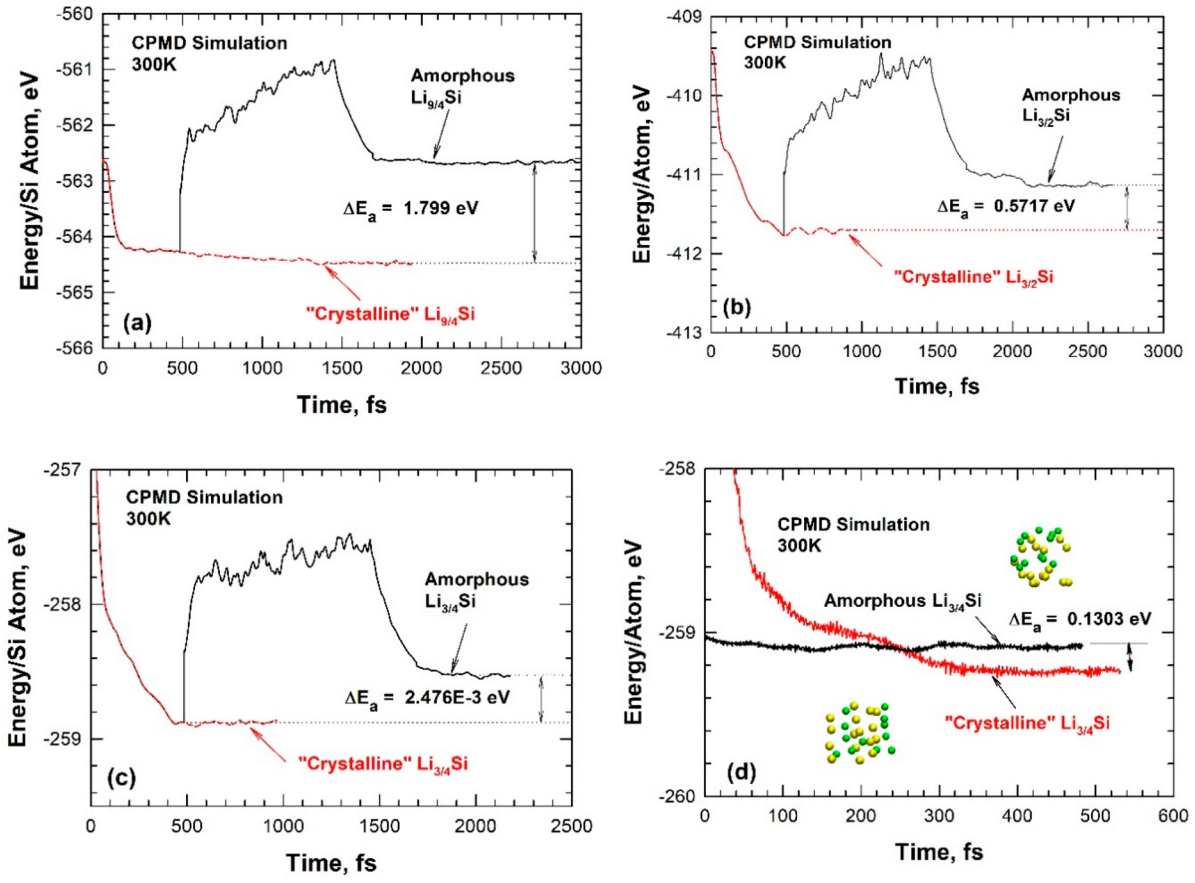

Figure 3. Energy/Si atom for "crystalline" Li_xSi produced by extraction of Li atoms from a supercell of $Li_{15}Si_4$ compared to a-Li_xSi produced by heating and quenching of the "crystalline" Li_xSi: (a) $Li_{9/4}Si$, (b) $Li_{3/2}Si$, (c) $Li_{3/4}Si$ (Li in the 48e sites), and (d) $Li_{3/4}Si$ (Li in the 12a sites) (yellow: Si; green: Li).

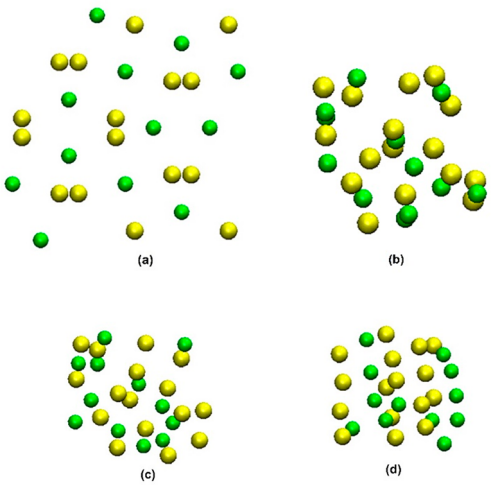

Figure 4. Structure of $Li_{3/4}Si$ after extraction of 48 Li atoms from $Li_{15}Si_4$ at various times of relaxation at 300 K: (a) 0, (b) 100, (c) 200, and (d) 400 fs. Rapid shrinkage of the unit cell occurs between (a) and (b) (yellow: Si; green: Li).

of formation are negative and become more negative with increasing unit cell volumes. The increasing negative energy of formation indicates increasing driving force for lithiation. The energy of formation for each a-Li_xSi compound is generally higher than that for the crystalline counterpart. For a-Li_3Si, the energy of formation is positive and is considerably higher than that for c-Li_3Si. Lithiation path c-L1 has been constructed to pass through all of the crystalline phases from c-Si to c-$Li_{15/4}Si$. There is a large gap between c-Li_3Si and c-$Li_{15/4}Si$, and path c-L1 goes between these two compounds and lies close to a-$Li_{15/4}Si$. In contrast, lithiation path a-L1 has been constructed to go through a-Si, a-$Li_{3/4}Si$, and a-$Li_{15/4}Si$, excluding a-$Li_{3/2}Si$, a-$Li_{9/4}Si$, and a-Li_3Si due to the much higher energies of the latter group. Path c-L1 is a slightly lower energy path compared to a-L1, as shown in Figure 5a.

Figure 5b shows a plot of the energy of formation for the Li_xSi compounds as a function of the Li content, x, for both the crystalline and amorphous compounds. For c-Li_xSi compounds, the energy of formation is negative and becomes more negative with increasing Li insertion. In contrast, the formation energy of a-Li_3Si is positive and is considerably higher than that for "c-Li_3Si", suggesting that the formation of a-Li_3Si is more difficult than that for "c-Li_3Si". Similarly, the formation energy of a-$Li_{9/4}Si$ is also higher than that of c-$Li_{9/4}Si$. The amorphization energy, E_a, for Li_3Si is 1.12 eV, while it is 1.799 eV for a-$Li_{9/4}Si$, as shown in Table 3. Lithiation path c-L1 is selected to go through the crystalline phases, while a-L1 connects those of a-Si, a-$Li_{3/4}Si$, and a-$Li_{15/4}Si$ but excludes those of a-$Li_{3/2}Si$, a-$Li_{9/4}Si$, and a-Li_3Si because of the high energies of formation the latter group. Figure 5b also presents results of the energy of formation for a-Li_xSi computed based on the ABINIT code[56] from Chevrier and Dahn.[36] The comparison in Figure 5b indicates that c-L1 is a lower-energy path compared to a-L1. Both c-L1 and a-L1

DOI: 10.1021/acs.jpcc.9b05933
J. Phys. Chem. C 2019, 123, 22775−22786

Table 3. Summary of the Computed Internal Energy of Compound (E_r)/Si Atom, Volume of Unit Cell (v) to the 1/3 Power, Number of Li Atoms (x_{Li}) in the Lithiated Compound, Energy of Formation (E_f), Amorphization Energy (E_a), and the Li-Atom Site (12a or 48e) within the Structure of c-$Li_{15}Si_4$[a]

material	x_{Li}	Li atom site	E_r/Si atom, eV	$\langle v\rangle^{1/3}$, Å	E_f, eV	E_a, eV
c-Si	n.a.		−106.7413	5.5290	n.a.	
Li	n.a.		−203.1904	3.5900	n.a.	
c-$Li_{15/4}Si$	3.75	a, e	−870.0786	10.7400	−1.3733	
a-$Li_{15/4}Si$	3.75	a, e	−869.8406	10.6700	−1.1383	0.235
c-Li_3Si	3	e	−717.1258	10.4393	−0.8133	
a-Li_3Si	3	e	−715.8740	9.6661	0.4385	1.120
c-$Li_{3/4}Si$	0.75	a	−259.2380	7.6469	−0.1039	
a-$Li_{3/4}Si$	0.75	a	−259.0824	7.5577	0.0517	0.1303
a-Si	0		−106.5533	5.5290	0.1880	0.188
a-$Li_{3/2}Si$	1.5	e	−411.5347	8.7083	−0.0078	0.5715
c-$Li_{3/2}Si$	1.5	e	−412.0937	8.7016	−0.5668	
a-$Li_{9/4}Si$	2.25	e	−563.5558	9.7820	0.3639	1.799
c-$Li_{9/4}Si$	2.25	e	−564.7201	9.0996	−0.8004	
a-$Li_{3/4}Si$	0.75	e	−259.2617	7.6798	−0.1276	0.002473
c-$Li_{3/4}Si$	0.75	e	−259.3920	7.5392	−0.2580	

[a]A prefix of "c-" indicates crystalline, while "a-" indicates amorphous.

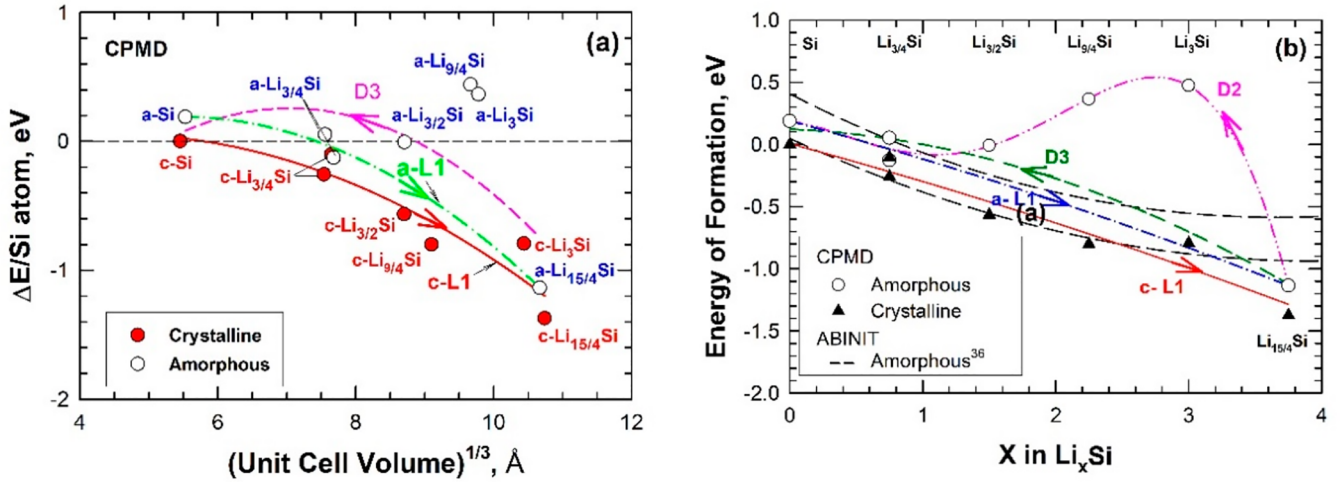

Figure 5. (a) Energy of formation for a-Si, c-Si, a-Li_xSi, and c-Li_xSi as a function of the unit cell volume to the 1/3 power. (b) Energy of formation of a-Li_xSi and c-Li_xSi as a function of the number, x, of Li atoms. Superimposed are lithiation path L1, and delithiation paths D1, D2, and D3. Some of the crystalline phases ($Li_{3/4}Si$, $Li_{3/2}Si$, and $Li_{9/4}Si$) may not be truly crystalline. The amorphous curves (dashed) are from Chevrier and Dahn.[36]

lie within the energy band reported by Chevier and Dahn,[36] except at high Li contents where $x > 3$. Figure 5b also presents two delithiation paths (D2, D3) that have been selected to include relevant phases on the basis of the energy of formation of individual compounds. In Figure 5b, the D2 path includes a-Li_3Si and a-$Li_{9/4}Si$, and it exhibits a high-energy path. For D3, this delithiation path is purposely selected to avoid the high-energy phases such as a-Li_3Si and a-$Li_{9/4}Si$ and to include only lower-energy phases such as a-$Li_{3/2}Si$, a-$Li_{3/4}Si$, and a-Si. By excluding a-Li_3Si and a-$Li_{9/4}Si$, the energy values of D3 are slightly higher than those of c-L1 or a-L1 but are considerably less than those of D2, as shown in Figure 5b.

3.3. Calculated Voltage Profile. The values for the elastic constants (C_{ij}) and bulk moduli (B) for Si and c-$Li_{15/4}Si$ calculated using CPMD are shown in Table 4. The computed elastic constants and bulk moduli are in good agreement with similar values reported in the literature and the experimental values.[57] Thus, the computed hydrostatic residual stresses were obtained on the basis of reasonable values of elastic constants and bulk moduli.

Table 4. Comparison of Computed and Experimental Values (from Reference 57) of Elastic Constants (C_{11}, C_{12}, and C_{44}) and Bulk Moduli (B) for c-Si and c-$Li_{15}Si_4$

elastic constants, GPa	predicted value	experimental value[57]
C_{11} (Si)	161.39	165
C_{12} (Si)	69.63	63
C_{44} (Si)	80.19	79.1
B (Si)	100.22	97
B ($Li_{15}Si_4$)	1.419	

To compute the open-circuit voltage, the internal energy change was determined via CPMD to be −1.373 eV, and the corresponding intercalation voltage was determined to be 0.366 V. To verify the CPMD results, WIEN2K[51] was also utilized to compute the various energy terms in eq 1. The corresponding values for WIEN2K[51] computations are −1.352 eV and 0.361 V. As summarized in Table 5, these values are comparable to those reported by Kubota et al.[34] using the VASP code.[50]

DOI: 10.1021/acs.jpcc.9b05933
J. Phys. Chem. C 2019, 123, 22775−22786

Table 5. Comparison of the Computed Free Energy Change (ΔE_r) and the Open-Circuit Intercalation Voltage for Lithiation of c-Si to c-$Li_{15}Si_4$

code	ΔE_r, eV	intercalation voltage (volt)
WIEN2K	−1.352	0.361
CPMD	−1.373	0.366
VASP	−1.136[27]	0.303[34]

The open-circuit potentials for other Li_xSi compounds were also computed using eq 2 or 5 without considering the effects of hydrostatic stresses, and the results are presented in Figure 6a. The computed open-circuit potentials are compared against experimental data from the literature obtained from lithiation of a-Si[36] as a function of the Si mole fraction, x, in the Li_xSi lithiation process. The different Li_xSi and Si states are presented as insets in Figure 6a, while the various reaction paths are presented in Figure 5 and Table 6.

When the effects of hydrostatic stresses are ignored, the CPMD simulation tends to overpredict the open-circuit voltage at a given Si mole fraction such that the entire theoretical curve appears to lie above the experimental curve, as seen in Figure 6a. In addition, the computed open-circuit potential is relatively insensitive to the Si mole fraction (x) and is different from experimental observations shown in Figure 6a.

To correct for the discrepancy, eq 8 was utilized to compute the open-circuit potential under the influence of the effect of hydrostatic stresses during lithiation and delithiation. A hydrostatic stress of −3 GPa was chosen for lithiation, and 3 GPa was chosen for delithiation. These values were motivated by previous computations by Lu et al.[45] who showed that the open−circuit potential during lithiation is negative but is positive during delithiation of Si. The value of 3 GPa was chosen based on the first-principles computational results performed in this study (not shown), which show that $Li_{15/4}Si$ remained elastic up to about 3 GPa under hydrostatic loading. The yield stress of a-Si was reported to range from 1.75 GPa in the lithiated state[3] to about 5.23 GPa in the unlithiated state[58] under uniaxial compression. The computed yield stress of 3 GPa is in good agreement with the reported values in the literature. Appropriate hydrostatic stresses for various x values during lithiation and delithiation were used to compute the entire OPC curve shown in Figure 6b. Yielding Si or Li_xSi is unlikely because the hydrostatic tensile stresses during delithiation were elastic and on the order of 1 GPa[3] and the fracture stress of Li_xSi increased from 2.7 GPa at x = 3.75 to 8.8 GPa at x = 0.25.[39] The computed open-circuit potentials are in good agreement with the experimental trend when the effect of hydrostatic stresses on the open-circuit potential are properly accounted for. As illustrated in Figure 6b, lithiation of Li_xSi is predicted to occur at decreasing lithiation potentials (ranging from 0.288 to 0.088 V vs Li/Li^+ for path L1-a to L1-f, e.g., see the last column of Table 6) when Li atoms are inserted into the 48e sites first and then the 12a sites. For this path, the energy decreases almost linearly with increasing Li insertion until the formation of $Li_{15/4}Si$ as parts of the free energy are spent in overcoming the compressive hydrostatic stresses associated with lithiation. Delithiation of Li from $Li_{15}Si_4$ can proceed in the reverse manner. Alternatively, delithiation can proceed via path D2-a to D2-d, which results in the formation of a-Li_xSi such as a-$Li_{9/4}Si$ and a-Li_3Si that are of higher energy states compared to the "crystalline" counterparts. The open-circuit potential is increased during delithiation as the process is aided by the hydrostatic tensile stresses generated during delithiation.

An important finding in Table 6 is that most of the lithiation and delithiation paths involving c-Si and a-Si lead to large volume changes. The volume changes are large for both the a-Li_xSi and c-Li_xSi compounds. In general, the volume change increases with increasing Li content, as shown in Table 6. Large hydrostatic tensile stresses are induced when the Li atoms are extracted from $Li_{15/4}Si$ during delithiation to Li_3Si and $Li_{9/4}Si$. The large volume changes occur at Li contents ($x \approx 2.25$) at which the lithiation process changes from a ledge mechanism to a two-phase process.[28] This finding suggests that the change in the lithiation mechanism at $x \approx 2.25$ may be stress-related. On the other hand, the high amorphization energy associated with a-Li_3Si and a-$Li_{9/4}Si$ suggests that the formation of these phases during delithiation is energetically unfavored and may not occur. Instead, a delithiation path such as D3 shown in Figure 5b, which involves the formation of Li_2Si or $Li_{1.5}Si$ without the formation of a-Li_3Si and $Li_{9/4}Si$, is

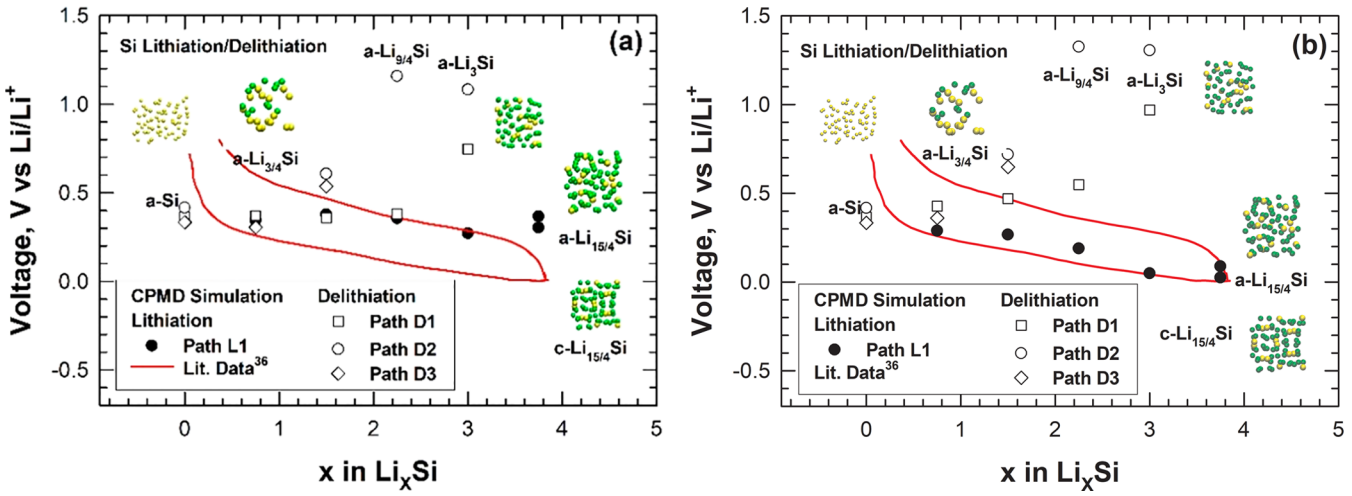

Figure 6. Open-circuit voltage as a function of Li atoms in Li_xSi: (a) open-circuit voltage computed via eq 5 without considering the effects of hydrostatic stresses and (b) open-circuit voltage computed via eq 8 to include the effects of hydrostatic stresses induced during lithiation and delithiation. Literature data are from Chevier and Dahn.[36]

DOI: 10.1021/acs.jpcc.9b05933
J. Phys. Chem. C 2019, 123, 22775−22786

Table 6. Summary of Computed Energy Changes (ΔE), the Open-Circuit Voltage (OCP and OCP*), Mole Fraction Change of Li, Volume, And Volume Change (Δvol) Associated with Various Lithiation and Delithiation Paths of c-Si and a-Si Anodes[a]

path	reaction	ΔE, eV	Δx_{Li}	OCP, V	x_{Li}	vol_i, A^3	vol_f, A^3	Δvol, %	OCP*, V
L1-a	c-Si + 3/4Li → c-$Li_{3/4}$Si	−0.25795	0.75	0.344	0.750	205.34	431.69	110.23	0.288
L1-b	c-Si + 3/2Li → c-$Li_{3/2}$Si	−0.5667785	1.5	0.378	1.500	237.22	658.87	177.75	0.267
L1-c	c-Si + 9/4Li → c-$Li_{9/4}$Si	−0.800395	2.25	0.356	2.250	269.10	753.47	180.00	0.189
L1-d	c-Si + 3Li → c-Li_3Si	−0.81329	3	0.271	3.000	300.98	1137.66	277.98	0.049
L1-e	c-Si + 15/4Li → a-$Li_{15/4}$Si	−1.136	3.75	0.303	3.750	332.86	1240.34	272.63	0.025
L1-f	c-Si + 15/4Li → c-$Li_{15/4}$Si	−1.373	3.75	0.366	3.750	332.86	1242.30	273.21	0.088
D1-a	c-$Li_{15/4}$Si → c-Li_3Si + 3/4Li	0.55999925	−0.75	0.747	3.000	1215.79	935.64	−23.04	0.969
D1-b	c-$Li_{15/4}$Si → c-$Li_{9/4}$Si + 3/2Li	0.5728935	−1.5	0.382	2.250	1215.79	817.23	−32.78	0.549
D1-c	c-$Li_{15/4}$Si → c-$Li_{3/2}$Si + 9/4Li	0.80651075	−2.25	0.358	1.500	1215.79	754.51	−37.94	0.470
D1-d	c-$Li_{15/4}$Si → c-$Li_{3/4}$Si + 3Li	1.1153361	−3	0.372	0.750	1215.79	559.21	−54.00	0.427
D1-e	c-$Li_{15/4}$Si → c-Si + 15/4Li	1.37328925	−3.75	0.366	0.000	1215.79	332.86	−72.62	0.366
D2-b	c-$Li_{15/4}$Si → a-Li_3Si + 3/4Li	0.81175925	−0.75	1.082	3.000	1215.79	935.02	−23.09	1.305
D2-c	c-$Li_{15/4}$Si → a-$Li_{9/4}$Si + 3/2Li	1.7371999	−1.5	1.158	2.250	1215.79	999.78	−17.77	1.325
D2-d	c-$Li_{15/4}$Si → a-$Li_{3/2}$Si + 9/4Li	1.36545695	−2.25	0.607	1.500	1215.79	756.03	−37.82	0.718
D2-a	c-$Li_{15/4}$Si → a-Si + 15/4Li	1.56128925	−3.75	0.416	0.000	1215.79	328.46	−72.98	0.416
D3-a	c-Li_3Si → a-$Li_{9/4}$Si + 3/4Li	1.17720065	−0.75	1.570	2.250	1137.66	967.90	−14.92	1.737
D3-b	c-Li_3Si → a-$Li_{3/2}$Si + 3/2Li	0.8054577	−1.5	0.537	1.500	1137.66	724.15	−36.35	0.648
D3-c	c-Li_3Si → a-$Li_{3/4}$Si + 9/4Li	0.68569585	−2.25	0.305	0.750	1137.66	548.59	−51.78	0.360
D3-d	c-Li_3Si → a-Si + 3Li	1.00129	−3	0.334	0. 000	1137.66	296.58	−73.93	0.334

[a]The OCP* values incorporate the effects of lithiation stresses, while the OCP values do not.

energetically favored and may be more likely to occur. Indeed, experimental observations indicate that delithiation of a-$Li_{15/4}$Si occurs through a two-phase reaction process with the formation of a-Li_2Si without the occurrence of a-Li_3Si and a-$Li_{9/4}$Si.[24,25,32] The notion of multiple possible delithiation paths is also supported by the experimental observations by J. W. Wang et al.[28] and Xu Wang et al.[31] that the delithiation paths and products varied with the charging rates. In particular, J. W. Wang et al.[28] observed a two-phase delithiation path involving Li_xSi with x being about 2.5 under high charge rates ($\gg$1C), while Xu Wang et al.[31] reported a single-phase delithiation path under slower charging rates (<1C).

4. DISCUSSION

In this investigation, the energies of formation of several a-Li_xSi compounds were computed by applying at elevated temperature (2500 K) a melting and rapid quenching technique to randomize atoms in a fully filled or a partially filled supercell of c-Li_xSi, followed by relaxation of the randomized cluster at ambient temperature. While there exists a possibility that the rapid quenching procedure may not render a truly random structure, the a-Li_xSi structures generated by the approach described in this investigation are expected to be highly randomized with fairly reproducible amorphization energy (ΔE_a) values because of the use a small time step (0.0483 fs), a high melting temperature (2500 K), a relatively long relaxation time (500−2000 fs), and a small energy change criterion (<1×10^{-5} eV) for the termination of the relaxation calculation. As a result of the small energy change criterion, the amorphization energy value is expected to have an accuracy better than 0.001 eV.

The current investigation identifies several metastable a-Li_xSi phases (a-Li_3Si, a-$Li_{9/4}$Si, and a-$Li_{3/2}$Si) that may be difficult to produce by delithiation experiments. Generated by a melting and rapid quenching computational scheme, these metastable phases are physically meaningful and relevant to the electrochemical delithiation processes in a-$Li_{15/4}$Si as some of these metastable phases are supported by evidence available in the literature. The formation of a-$Li_{3/2}$Si during delithiation of Si has recently been demonstrated by Jung et al.[46] on the basis of ReaxFF MD simulation of the delithiation process in Si NWs. A two-phase lithiation region of a-Si and a-$Li_{2.5}Si$[29] was observed by J. W. Wang et al.[28] A two-phase delithiation region of a-Li_2Si and a-$Li_{15/4}$Si was reported by Li and Dahn[25] and later confirmed by Gauthier et al.[32] The current study also showed that the energy of formation of c-Li_3Si is considerably lower than that of a-Li_3Si but is about the same as that of a-$Li_{15/4}$Si. The occurrence of Li_3Si on isolated delithiated Si particles has been identified by Danet et al.[30] using valence electron energy loss spectroscopy and by Radvanyi et al.[59] using Auger electron spectroscopy. Unfortunately, the crystallinity of the Li_3Si phase was not determined. It should also be noted that c-$Li_{15/4}$Si is a metastable compound that was observed during lithiation of Si, but this phase is not expected based on the published Li−Si phase diagram.[1]

The first-principles computational results indicate that c-$Li_{15}Si_4$ and all of the intermediate "crystalline" phases formed by extracting Li atoms from c-$Li_{15}Si_4$ exhibit lower energy states than the amorphous counterparts formed by heating and rapid quenching. These energy states can be utilized to infer the lithiation and delithiation paths for Si if one assumes that these energy changes are equal in magnitude but have opposite signs. On the basis of this assumption, the first-principles computation results suggest that Li ion insertion into Si may occur through a process resembling the filling of the 48e sites of the simple cubic structure of the $Li_{15}Si_4$ unit cell first to form the compositions $Li_{3/4}Si$, $Li_{3/2}Si$, $Li_{9/4}Si$, and Li_3Si. Filling the 12a sites by Li would result in the formation of a-$Li_{15/4}$Si or c-$Li_{15/4}$Si because the energy state of Li_3Si is higher than that of a-$Li_{15/4}$Si, which, in turn, is higher than that of c-$Li_{15/4}$Si. This lithiation path is consistent with experimental observations[23,24] that indicated the formation of a-$Li_{15/4}$Si first, followed by congruent transformation of a-$Li_{15/4}$S to c-$Li_{15/4}$Si. Experimental observations[23,24] did not detect the formation of any intermediate crystalline phases such as $Li_{3/4}Si$, $Li_{3/2}Si$, $Li_{9/4}Si$, and Li_3Si. A possible explanation is that a-Li_xSi is favored over

DOI: 10.1021/acs.jpcc.9b05933
J. Phys. Chem. C 2019, 123, 22775−22786

the "crystalline" phases due to kinetic constraints imposed by the lithiation rate. Thus, the a-L1 path is favored over c-L1 (Figure 5a). Recent ReaxFF MD simulations[47] and experimental works[28,31] have shown that the lithiation mechanism in a-Si depends on the charging rate. For example, a two-phase reaction involving a-Si and a-$Li_{2.5}Si$ was observed at high charging rates (≫1C),[28] while a single-phase lithiation of a-Li_xSi was observed at conventional charging rates (<1C). In addition, the transformation of c-$Li_{15/4}Si$ to a-$Li_{15/4}Si$ was observed only at voltages below 30−60 mV vs Li/Li^+. Extrapolating from this observation, it is possible that the "crystalline" intermediate phases might able to form only at low voltages (e.g., below 30 mV), thereby limiting if not preventing their occurrence in conventional lithiation experiments.

Several delithiation paths have been considered to include both crystalline and amorphous compounds in the delithiation process. The predicted delithiation paths in Si are more complicated when a-Li_3Si is involved because it has a higher energy state than c-Li_3Si and lithiated compounds. The lowest-energy path corresponds to the one that is identical to the lithiation path (c-L1) but operates in reverse order, which is designated D1 in Table 6. Both c-L1 and D1 take place at a relatively constant range of open-circuit potentials (∼0.35 eV) (Figure 6a). The inclusion of higher-energy amorphous compounds such as a-Li_3Si and a-$Li_{9/4}Si$ resulted in delithiation path D2 that exhibited a higher open-circuit potential. The experimental observations of the absence of a-Li_3Si and a-$Li_{9/4}Si$ during delithiation of a-$Li_{15/4}Si$ may be attributed to the high amorphization energy of these compounds. Instead of D2, a delithiation path such as D3 shown in Figure 5b that involves the formation of a-$Li_{3/2}Si$, a-$Li_{3/4}Si$, and a-Si without the formation of a-Li_3Si and a-$Li_{9/4}Si$ is more likely based on the energetic ground. Such a path is also consistent with two key findings: (1) a two-phase delithiation process involving c-Si and a-Li_xSi at compositions below a-$Li_{3/2}Si$ observed by Jung et al.[46] in their ReaxFF MD simulations and (2) experimental observations of the formation of a-Li_2Si in a two-phase reaction during delithiation of a-$Li_{15/4}Si$.[24,25,31] The computed values of the open-circuit potential are generally higher than those observed experimental curves, and the shape of the curve is also different when the effect of hydrostatic tensile stresses are ignored in the calculation of the open-circuit potential. Once included in the calculation, the computed open-circuit potentials are in good agreement with experimental observations, as shown in Figure 6b. Thus, the current finding supports the previous results by Lu et al.[45] that parts of the voltage hysteresis of Li-ion batteries with Si anodes are caused by the mechanical stresses induced during lithiation and delithiation.

The computed volume changes associated with individual steps during the various lithiation and delithiation paths are presented in the fifth column of Table 6. During lithiation, the volume changes at various steps are in the range of 110−273%, and the corresponding hydrostatic stresses are compressive. In contrast, the volume changes associated with individual steps in the various delithiation paths are negative, ranging from −17.73 to −73.93% due to volume contraction of the delithiated compounds, as can be seen in Figure 4a,b. The hydrostatic stresses that correspond to the negative volume changes are tensile, and these induced tensile stresses are sufficiently high to cause fracture of the delithiated phases or compounds.

The results of this investigation suggest that multiple paths are feasible during delithiation of c-$Li_{15/4}Si$ or a-$Li_{15/4}Si$ based on energetic consideration of various a-Li_xSi compounds when $1.5 < x < 3.75$. In comparison, ReaxFF MD simulations of the delithiation behavior of a Si thin film by Kim et al.[47] indicated that the delithiation path of a-Li_xSi is dependent on the delithiation rate. According to Kim et al.,[47] fast delithiation led to the formation of porosity inside of a-Li_xSi, while slow delithiation led to the formation of a-$Li_{1/5}Si$ with a volume expansion of 44%. Thus, multiple delithiation paths of a-$Li_{15/4}Si$ can result from two sources: (a) a thermodynamic driving force (energetics in this study) that dictates which compounds can be formed and (2) a kinetic driving force (Kim et al.[47]) that dictates the compounds, crystallinity (crystalline vs amorphous), and structures (porosity etc.) of the reaction products.

5. CONCLUSIONS

The conclusions reached as the results of this investigation are as follows:

- The lithiation and delithiation processes in Si can be modeled using the first-principles MD code based on the CPMD method.
- On the basis of the energetics, this lithiation process in Si is predicted to follow a path (c-L1) in which the structure resembles the formation of relaxed "crystalline" phases of $Li_{3/4}Si$, $Li_{3/2}Si$, $Li_{9/4}Si$, Li_3Si, and $Li_{15/4}Si$ by filling the 48e sites and then the 12a sites within the $I\bar{4}3d$ space group. The experimental path appears to follow the a-L1 path, which includes amorphous counterparts of these phases but excludes a-Li_3Si due to kinetics constraints and high amorphization energy of a-Li_3Si. This lithiation path (a-L1) is supported by the close correspondence between the calculated lithiation voltages, including the effects of hydrostatic stresses, and experimental values obtained from electrochemical measurements.
- Lithiation of Si is predicted to occur at a relatively constant potential in the absence of lithiation stresses, but the corresponding volume change is predicted to increase with increasing number of Li ions inserted. The presence of hydrostatic stresses accompanying lithiation/delithiation alters the shape of the calculated open-circuit potential vs capacity curve.
- Delithiation of c-$Li_{15/4}Si$ can occur via multiple paths due to the formation of high energy state a-Li_xSi compounds with the Li_3Si and $Li_{9/4}Si$ compositions. The formation of these amorphous compounds during delithiation leads to increasing open-circuit potentials with increasing Li ions extracted. Large volume shrinkage is predicted to occur for all delithiation paths.
- The observation of a two-phase (a-Li_2Si and c-$Li_{15/4}Si$) field during delithiation may be attributed to a large amorphization energy of Li_3Si and $Li_{9/4}Si$. The amorphous energy of $Li_{9/4}Si$ is also shown to vary with the sites where the Li atoms are located in the partially filled structure.
- The change in the lithiation process from a ledge mechanism to a two-phase mechanism at $x \approx 2.25$ may be stress-related and may be attributed to the large volume change and the high amorphization energy associated with a-Li_3Si and a-$Li_{9/4}Si$.

DOI: 10.1021/acs.jpcc.9b05933
J. Phys. Chem. C 2019, 123, 22775−22786

AUTHOR INFORMATION

Corresponding Authors

*E-mail: kchansatx@icloud.com.
*E-mail: candace.chan@asu.edu.

ORCID

Kwai S. Chan: 0000-0002-8838-1551
Candace K. Chan: 0000-0003-4329-4865

Notes

The authors declare no competing financial interest.

ACKNOWLEDGMENTS

This work was supported by the Internal Research and Development Program (Project No. 18.R9890) of the Southwest Research Institute (SwRI). The contribution of C.K.C. was supported by the National Science Foundation through Grant No. DMR-1206795 and startup funds from the Fulton Schools of Engineering, Arizona State University (ASU). The first-principles computations were performed at the Texas Advanced Computing Center of the TerraGrid network.

REFERENCES

(1) Wen, C. J.; Huggins, R. A. Chemical Diffusion in Intermediate Phases in the Lithium-Silicon System. *J. Solid State Chem.* **1981**, *37*, 271−278.

(2) Timmons, A.; Dahn, J. R. Isotropic Volume Expansion of Particles of Amorphous Metallic Alloys in Composite Negative Electrodes for Li-Ion Batteries. *J. Electrochem. Soc.* **2007**, *154*, A444−A448.

(3) Sethuraman, V. A.; Chon, M. J.; Shimshak, M.; Srinivasan, V.; Guduru, P. R. In Situ Measurements of Stress Evolution in Silicon Thin Films During Electrochemical Lithiation and Delithiation. *J. Power Sources* **2010**, *195*, 5062−5066.

(4) Lewis, R. B.; Timmons, A.; Mar, R. E.; Dahn, J. R. In situ AFM Measurements of the Expansion and Contraction of Amorphous Sn-Co-C Films Reacting With Lithium. *J. Electrochem. Soc.* **2007**, *154*, A213−A261.

(5) Timmons, A.; Dahn, J. R. In Situ Optical Observations of Particle Motion in Alloy Negative Electrodes for Li-Ion Batteries. *J. Electrochem. Soc.* **2006**, *153*, A1206−A1210.

(6) Beattie, S. D.; Larcher, D.; Morcrette, M.; Simon, B.; Tarascon, J. M. Si Electrodes for Li-Ion Batteries − a New Way to Look at an Old Problem. *J. Electrochem. Soc.* **2008**, *155*, A158−A163.

(7) Eom, J. Y.; Park, J. W.; Kwon, H. S.; Rajendran, S. Electrochemical Insertion of Lithium into Multiwalled Carbon Nanotube/Silicon Composites Produced by Ballmilling. *J. Electrochem. Soc.* **2006**, *153*, A1678−A1684.

(8) Zhang, Y.; Zhang, X. G.; Zhang, H. L.; Zhao, Z. G.; Li, F.; Liu, C.; Cheng, H. M. Composite Anode Material of Silicon/Graphite/Carbon Nanotubes for Li-Ion Batteries. *Electrochim. Acta* **2006**, *51*, 4994−5000.

(9) Zhang, Y.; Zhao, Z. G.; Zhang, X. G.; Zhang, H. L.; Li, F.; Liu, C.; Cheng, H. M. Pyrolytic Carbon-Coated Silicon/Carbon Nanotube Composites: Promising Application for Li-Ion Batteries. *Int. J. Nanomanuf.* **2008**, *2*, 4−15.

(10) Huggins, R. A.; Nix, W. D. Decrepitation Model for Capacity Loss during Cycling of Alloys in Rechargeable Electrochemical Systems. *Ionics* **2000**, *6*, 57−63.

(11) Ryu, J. H.; Kim, J. W.; Sung, Y.-E.; Oh, S. M. Failure Modes of Silicon Powder Negative Electrode in Lithium Secondary Batteries. *Electrochem. Solid-State Lett.* **2004**, *7*, A306−A309.

(12) Graetz, J.; Ahn, C. C.; Yazami, R.; Fultz, B. Highly Reversible Lithium Storage in Nanostructured Silicon. *Electrochem. Solid-State Lett.* **2003**, *6*, A194−A197.

(13) Takamura, T.; Ohara, S.; Uehara, M.; Suzuki, J.; Sekine, K. A Vacuum Deposited Si Film Having a Li Extraction Capacity Over 2000 mAh/g With a Long Cycle Life. *J. Power Sources* **2004**, *129*, 96−100.

(14) Kim, H.; Han, B.; Choo, J.; Cho, J. Three-Dimensional Porous Silicon Particles for Use in High-Performance Lithium Secondary Batteries. *Angew. Chem., Int. Ed.* **2008**, *47*, 10151.

(15) Green, M.; Fielder, E.; Scrosati, B.; Wachtler, M.; Moreno, J. S. Structured Silicon Anodes for Lithium Battery Applications. *Electrochem. Solid-State Lett.* **2003**, *6*, A75−A79.

(16) Chan, C. K.; Peng, H.; Liu, G.; McIlwrath, K.; Zhang, X. F.; Huggins, R. A.; Cui, Y. High-Performance Lithium Battery Anodes Using Silicon Nanowires. *Nat. Nanotechnol.* **2008**, *3*, 31−35.

(17) Cui, L.-F.; Ruffo, R.; Chan, C. K.; Peng, H.; Cui, Y. Crystalline-Amorphous Core-Shell Silicon Nanowires for High Capacity and High Current Battery Electrodes. *Nano Lett.* **2009**, *9*, 491−495.

(18) Wu, H.; Chan, G.; Choi, J. W.; Ryu, I.; Yao, Y.; McDowell, M. T.; Lee, S. W.; Jackson, A.; Yang, Y.; Hu, L.; et al. Stable Cycling of Double-Walled Silicon Nanotube Battery Anodes Through Solid-Electrolyte Interphase Control. *Nat. Nanotechnol.* **2012**, *7*, 310−315.

(19) Wu, H.; Cui, Y. Designing Nanostructured Si Anodes for High Energy Lithium Ion Batteries. *Nano Today* **2012**, *7*, 414−429.

(20) McDowell, M. T.; Lee, S. W.; Nix, W. D.; Cui, Y. 25th Anniversary Article: Understanding the Lithiation of Silicon and Other Alloying Anodes for Lithium-Ion Batteries. *Adv. Mater.* **2013**, *25*, 4966−4985.

(21) Beaulieu, L. Y.; Hatchard, T. D.; Bonakdarpour, A.; Fleischauer, M. D.; Dahn, J. R. Reaction of Li with Alloy Thin Films Studied by In Situ AFM. *J. Electrochem. Soc.* **2003**, *150*, A1457−A1464.

(22) Obrovac, M. N.; Christensen, L. Structural Changes in Silicon Anodes during Lithium Insertion/Extraction. *Electrochem. Solid-State Lett.* **2004**, *7*, A93−A96.

(23) Obrovac, M. N.; Krause, L. J. Reversible Cycling of Crystalline Silicon Powder. *J. Electrochem. Soc.* **2007**, *154*, A103−A108.

(24) Hatchard, T. D.; Dahn, J. R. In Situ XRD and Electrochemical Study of the Reaction of Lithium with Amorphous Silicon. *J. Electrochem. Soc.* **2004**, *151*, A838−A842.

(25) Li, J.; Dahn, J. R. An In Situ X-ray Diffraction Study of the Reaction of Li with Crystalline Si. *J. Electrochem. Soc.* **2007**, *154*, A156−A161.

(26) Li, J.; Smith, A.; Sanderson, R. J.; Hatchard, T. D.; Dunlap, R. A.; Dahn, J. R. In-situ ^{119}Sn Mössbauer effect study of the reaction of lithium with Si using a Sn probe. *J. Electrochem. Soc.* **2009**, *156*, A283−A288.

(27) Liu, X. H.; Wang, J. W.; Huang, S.; Fan, F.; Huang, X.; Liu, Y.; Krylyuk, S.; Yoo, J.; Dayeh, S. A.; Davydov, A. V.; Mao, S. X.; Picraux, S. T.; Zhang, S.; Li, J.; Zhu, T.; Huang, J. Y. In Situ Atomic Scale Imaging of Electrochemical Lithiation in Silicon. *Nat. Nanotechnol.* **2012**, *7*, 749−756.

(28) Wang, J. W.; He, Y.; Fan, F.; Liu, X. H.; Xia, S.; Liu, Y.; Harris, C. T.; Li, H.; Huang, J. Y.; Mao, S. X.; Zhu, T. Two-Phase Electrochemical Lithiation in Amorphous Silicon. *Nano Lett.* **2013**, *13*, 709−713.

(29) Limthongkul, P.; Jang, Y.-I.; Dudney, N. J.; Chiang, Y.-M. Electrochemically-Driven Solid-State Amorphization in Lithium-Silicon Alloys and Implications for Lithium Storage. *Acta Mater.* **2003**, *51*, 1103−1113.

(30) Danet, J.; Brousse, T.; Rasim, K.; Guyomard, D.; Moreau. Valence Electron Energy-Loss Spectroscopy of Silicon Negative Electrodes for Lithium Batteries. *Phys. Chem. Chem. Phys.* **2010**, *12*, 220−226.

(31) Wang, X.; Singh, S. S.; Ma, T.; Lv, C.; Chawla, N.; Jiang, H. Quantifying Electrochemical Reactions and Properties of Amorphous Silicon in a Conventional Lithium-ion Battery Configuration. *Chem. Mater.* **2017**, *29*, 5831−5840.

(32) Gauthier, M.; Danet, J.; Lestriez, B.; Roue, L.; Guyomard, D.; Moreau, P. Nanoscale Compositional Changes During First Delithiation of Si Negative Electrodes. *J. Power Sources* **2013**, *227*, 237−242.

DOI: 10.1021/acs.jpcc.9b05933
J. Phys. Chem. C 2019, 123, 22775−22786

(33) Aydinol, M. K.; Ceder, G. First-Principles Prediction of Insertion Potentials in Li-Mn Oxides for Secondary Li Batteries. *J. Electrochem. Soc.* **1997**, *144*, 3832−3835.
(34) Kubota, Y.; Escaño, M. C. S.; Nakanishi, H.; Kasai, H. Crystal and Electronic Structure of $Li_{15}Si_4$. *J. Appl. Phys.* **2007**, *102*, 053704.
(35) Chevrier, V. L.; Zwanziger, J. W.; Dahn, J. R. First Principles Studies of Silicon as a Negative Electrode Materials for Lithium-Ion Batteries. *Can. J. Phys.* **2009**, *87*, 625−632.
(36) Chevrier, V. L.; Dahn, J. R. First Principles Model of Amorphous Silicon Lithiation. *J. Electrochem. Soc.* **2009**, *156*, A454−A458.
(37) Chevrier, V. L.; Dahn, J. R. First Principles Studies of Disordered Lithiated Silicon. *J. Electrochem. Soc.* **2010**, *157*, A392−A398.
(38) Kim, H.; Chou, C.-Y.; Ekerdt, J. G.; Hwang, G. S. Structure and Properties of Li-Si Alloys: A First Principles Study. *J. Phys. Chem. C* **2011**, *115*, 2514−2521.
(39) Sitinamaluwa, H. S.; Wang, M. C.; Will, G.; Senadeera, W.; Zhang, S.; Yan, C. Lithium Concentration Dependent Structure and Mechanics of Amorphous Silicon. *J. Appl. Phys.* **2016**, *119*, 245103.
(40) Zhang, Q.; Zhang, W.; Wan, W.; Cui, Y.; Wang, E. Lithium Insertion in Silicon Nanowires: An ab initio Study. *Nano Lett.* **2010**, *10*, 3243−3249.
(41) Zhang, Q.; Cui, Y.; Wang, E. First-Principles Approaches to Simulate Lithiation in Silicon Electrodes. *Modell. Simul. Mater. Sci. Eng.* **2013**, *21*, 074001.
(42) Wan, W.; Zhang, Q.; Cui, Y.; Wang, E. First Principles Study of Lithium Insertion in Bulk Silicon. *J. Phys.: Condens. Matter* **2010**, *22*, 415501.
(43) Chan, M. K. Y.; Wolverton, C.; Greeley, J. P. First Principles Simulations of the Electrochemical Lithiation and Delithiation of Faceted Crystalline Silicon. *J. Am. Chem. Soc.* **2012**, *134*, 14362−14374.
(44) Pan, J.; Zhang, Q.; Li, J.; Beck, M. J.; Xiao, X.; Cheng, Y.-T. Effects of Stress on Lithium Transport in Amorphous Silicon Electrodes for Lithium-Ion Batteries. *Nano Energy* **2015**, *13*, 192−199.
(45) Lu, B.; Song, Y.; Zhang, Q.; Pan, J.; Cheng, Y.-T.; Zhang, J. Voltage Hysteresis of Lithium Ion Batteries Caused by Mechanical Stress. *Phys. Chem. Chem. Phys.* **2016**, *18*, 4721−4727.
(46) Jung, H.; Lee, M.; Yeo, B. C.; Lee, K.-R.; Han, S. S. Atomistic Observation of the Lithiation and Delithiation Behaviors of Silicon Nanowires Using Reactive Molecular Dynamics Simulations. *J. Phys. Chem. C* **2015**, *119*, 3447−3455.
(47) Kim, K. J.; Wortman, J.; Kim, S.-Y.; Qi, Y. Atomistic Simulation Derived Insight on the Irreversible Structural Changes of Si Electrode during Fast and Slow Delithiation. *Nano Lett.* **2017**, *17*, 4330−4338.
(48) *CPMD*, version 3.13, IBM Corp 1990−2008; MPI für Festkörperforschung Stuttgart, 1997−2001; http://www.cpmd.org.
(49) Car, R.; Parrinello, M. Unified Approach for Molecular Dynamics and Density-Functional. *Phys. Rev. Lett.* **1985**, *55*, 2471−2474.
(50) Kresse, G.; Hafner. Ab Initio Molecular Dynamics for Liquid Metals. *Phys. Rev. B: Condens. Matter Mater. Phys.* **1993**, *47*, 558−561.
(51) Blaha, P.; Schwarz, K.; Madsen, G.; Kvasnicka, D.; Luitz, J. *WIEN2K User's Guide*; Vienna University of Technology: Vienna, 2001.
(52) Yin, M. T.; Cohen, M. L. Microscopic Theory of the Phase Transformation and Lattice Dynamics of Si. *Phys. Rev. Lett.* **1980**, *45*, 1004−1007.
(53) Zunger, A. Ground State Properties of Crystalline Silicon in a Density-Functional Pseudopotential Approach. *Phys. Rev. B: Condens. Matter Mater. Phys.* **1980**, *21*, 4785−4790.
(54) *Lithium*. http://www.infoplease.com/periodictable.php?id=3 (2019).
(55) Huggins, R. A. Lithium Alloy Negative Electrodes. *J. Power Sources* **1999**, *81*−*82*, 13−19.
(56) Torrent, M.; Jollet, F.; Bottin, F.; Zerah, G.; Gonze, X. Lithium Alloy Negative Electrodes. *Comput. Mater. Sci.* **2008**, *42*, 337−351.
(57) Wei, S.; Allan, D. C.; Wilkins, J. W. Elastic Constants of a Si/Ge Superlattice and of Bulk Si and Ge. *Phys. Rev. B: Condens. Matter Mater. Phys.* **1992**, *46*, 12411−12417.
(58) Follstaedt, D. M.; Knapp, J. A.; Myers, S. M. Mechanical Properties of Ion-Implanted Amorphous Silicon. *J. Mater. Res.* **2004**, *19*, 338−346.
(59) Radvanyi, E.; De Vito, E.; Porcher, W.; Danet, J.; Desbois, P.; Colin, J.-F.; Larbi, S. J. S. Study of Lithiation Mechanisms in Silicon Electrodes by Auger Electron Spectroscopy. *J. Mater. Chem. A* **2013**, *1*, 4956−4965.

DOI: 10.1021/acs.jpcc.9b05933
J. Phys. Chem. C 2019, 123, 22775−22786